Chapter 4

Electrospun Poly(Ethylene Oxide) Fibers Reinforced with Poly (Vinylpyrrolidone) Polymer and Cellulose Nanocrystals

Qinglin Wu, Changtong Mei, Xiuqiang Zhang, Tingzhou Lei, Zhen Zhang and Meichun Li

Additional information is available at the end of the chapter

http://dx.doi.org/10.5772/intechopen.76392

Abstract

Green poly(ethylene oxide) (PEO)/cellulose nanocrystals (CNCs)/poly(vinylpyrrolidone) (PVP) composites were prepared via electrospinning technique. The use of PVP and/or CNCs improved the overall thermal stability and mechanical properties of the PEO fibers. A strong synergistic reinforcing effect was achieved when PVP polymer and CNCs were combined in the composite. This synergistic reinforcement was accompanied with the formation of unique fiber-bead-fiber morphology. The beads were elongated and orientated along the applied force direction during tensile testing, providing an energy dissipation mechanism and a positive reinforcement effect. The combination of CNCs with PVP induced special chemical interactions, and distracted the interactions between PVP and PEO. As a result, the crystallinity of PEO was increased in the system, which also helped enhance fiber properties. The approach developed in this work offers a new way for reinforcing electrospun PEO-based composite fibers for sustainable green composite development.

Keywords: electrospinning, cellulose nanocrystals, reinforcing mechanisms, poly(ethylene oxide), poly(vinylpyrrolidone), green composites

1. Introduction

Currently, fabricating "green polymeric materials" that are environmentally friendly has received much attention in academic and industrial research [1–3]. However, one drawback

is relatively low strength of these biopolymers, which restricts their wide use for replacing synthetic polymers [4, 5]. One effective way to improve their strength and commercial use potential is to incorporate nano-sized reinforcement into the polymeric matrix [6–8]. Among the nano-fillers, cellulose nanocrystals (CNCs) have been considered as a competitive candidate, because of their high strength and Young's modulus [6, 9]. In addition, CNCs are inherently renewable, biodegradable, and biocompatible, leading to long-term sustainability [10, 11].

Poly(ethylene oxide) (PEO), as a nontoxic, biodegradable, and biocompatible polymer, has received tremendous attention in biomedical field [12, 13]. PEO-water solution system can be used to prepare nanofibers via electrospinning technique [6, 14, 15] for bone regeneration [16], drug release delivery [17], and adsorption of ions [18]. However, low mechanical strength of electrospun PEO nanofibers generally limits their application. To reinforce PEO nanofibers without decreasing their biodegradability and biocompatibility, green materials such as CNCs and cellulose nanofibers (CNFs) have been recently investigated. Zhou et al. [6] found that in the PEO/CNC binary nanocomposite system, CNCs can be highly aligned under high electrostatic fields, and induced heterogeneous microstructures regarding the uniformity of fiber size, which resulted in a considerable increase in mechanical strength. In another study [14], both CNCs and cellulose nanofibers (CNFs) were used to reinforce electrospun PEO nanofibers and CNFs exhibited a higher reinforcing efficiency, which was attributed to the unique shish-kebab-like crystalline structures formed within the nanofibers. The reinforcing effect of CNCs for PEO composite fibers needs to be further elucidated to understand their specific role in the composite.

Similar as PEO and CNCs, poly(vinylpyrrolidone) (PVP) is also biodegradable and biocompatible, and has been widely used in biomedical areas [19]. The introduction of PVP to the PEO-CNC system can offer some unique properties without deteriorating the green nature of PEO/CNC system. PVP is a rigid polymer with a glass transition temperature of 160°C [20]. Its higher rigidity in comparison with that of PEO makes it possible to serve as a reinforcement additive. PVP is also an amorphous polymer, which can influence the crystallization of PEO. For semi-crystalline polymers like PEO, its mechanical properties strongly depend upon its crystalline characteristics [21]. Therefore, it is possible to tailor mechanical properties of the material by using PVP in the composite. The carbonyl group in the molecular structure of PVP can work as the proton acceptor, which is prone to chemically interact with the proton in hydroxyl group (–OH) [22]. Considering the –OH groups in the molecular structure of PEO and CNCs, the addition of PVP can possibly contribute to special chemical interactions, which is also beneficial to the reinforcement [23].

Thus, it is of significant interest to incorporate PVP to the PEO-CNC composite via electrospinning technique for tailoring the mechanical properties of the composite system. Herein, electrospun PEO nanofiber mats reinforced with different contents of PVP and CNCs were prepared and a synergistic reinforcing effect was demonstrated in the ternary composites. Rheological properties of the electrospinning materials, thermal stability, crystallization, mechanical properties and morphology of the electrospun mats were investigated. An in-depth study on the reinforcing mechanism was presented.

http://dx.doi.org/10.5772/intechopen.76392

2. Experimental

2.1. Materials

PEO powder (M_v = 900,000 g/mol) was purchased from Sigma-Aldrich [St. Louis, MO]. PVP (K-30) was provided by Xilong Chemical Reagent Co. Ltd (Guangdong, China). The CNCs were extracted from the cellulose powder provided by Nippon Paper Chemicals Co., LTD (W-50 grade of KC Flock, Tokyo, Japan). In brief, acid hydrolysis of the wood powder with 64 wt% H_2SO_4 followed by high-pressure homogenization was used as described in our previous paper [10]. The specific dimensions of CNCs were 149 in length and 9 nm in diameter, respectively [10]. The prepared CNC suspensions were freeze-dried to get the dry CNC materials.

2.2. Electrospinning

To prepare the PEO/PVP/CNCs suspensions for electrospinning, predetermined amount of PEO, PVP and freeze-dried CNCs were mixed with distilled water, and the mixture was magnetically stirred for several hours, followed by ultrasonic treatment. The total polymeric concentration (i.e., PEO/PVP) was kept constant at 3 wt% for all solutions and suspensions. The weight percentages of PEO, PVP and CNCs were varied for different composite systems (**Table 1**). The prepared samples were designated as PxCy, where x and y represent the dosages of PEO/PVP (polymer) and CNCs, respectively, in part-per-hundred (phr). The prepared materials were loaded in a 5-ml BD plastic syringe with a 25 gauge stainless steel needle. A Chemyx Fusion 100 syringe pump (Stafford, TX) was used to feed the material with controlled feeding rates. A high voltage (15 KV) was applied between the needle and grounded aluminum fiber collector. The fiber collector was covered with a piece of aluminum foil pretreated with a small amount of silicon oil for better fiber mat release. After the electrospinning process, the mats with a thickness around 0.1 mm were removed from the collector plate and vacuum-dried at 40°C for 6 h before characterization.

Composite material type	Polymer system[a]		Reinforcing agent[b]
	PEO (PHR)	PVP (PHR)	CNC (PHR)
P100	100	0	0
P100C5	100	0	5
P90	90	10	0
P90C5	90	10	5
P80	80	20	0
P80C5	80	20	5

[a]PHR: part-per-hundred; Total polymer system (PEO/PVP) made up 100 PHR.
[b]CNC was in relation to the total polymer in the system in PHR.

Table 1. Formulation information of different electrospun PEO-PVP-CNC composite fiber mat systems.

2.3. Characterizations

Rheological properties of the electrospinning solutions/suspensions were investigated using an AR2000ex Rheometer (TA Instruments, New Castle, DE). A 40 mm cone-plate geometry with a cone angle of 1°59′42″ and 52 μm truncation was used for both flow and oscillatory measurements. The testing temperature was kept at 25°C using a temperature-regulated Peltier plate device. In order to avoid water evaporation from test samples, a solvent trap was used to seal the gap between the top cone-plate geometry and bottom Peltier plate. The moat on the top of the trap was filled with silicon oil. For flow measurement, steady shear rates applied varied within 1–100 s^{-1}. With regard to the oscillatory measurement, the angular frequency range was 0.05–100 s^{-1} and the strain was selected to be 50%, which was within the linear viscoelastic region. Fourier transform infrared (FTIR) spectra of the electrospun mats were tested using a Bruker FTIR analyzer (Tensor-27, Bruker Optics, Billerica, MA) with an attenuated total reflectance (ATR) mode. Thirty two scans combined with a spectral range of 4000–600 cm^{-1} were used. Differential scanning calorimetry (DSC) was performed with a TA Q200 DSC system (TA Instruments-Waters LLC, New Castle, DE). Each sample of about 2–6 mg was tested in a hermetic aluminum pan under 40 ml/min nitrogen flow. In order to eliminate any possible thermal history, the samples were first heated to 180°C at a heating rate of 40°C/min. Then, the samples were quickly quenched to −90°C to freeze polymeric chains in the material. The samples were then heated to 180°C at 10°C/min, equilibrated at 180°C for 1 min and cooled down to −40°C at 10°C/min. Thermogravimetric analysis (TGA) was carried out using a Q50 TG analyzer (TA Instruments-Waters LLC, New Castle, DE). All the tests were carried out under nitrogen flow (40 ml/min) in the temperature range of 50–600°C at 10°C/min. X-ray diffraction (XRD) measurements were carried out using a PANalytical empyrean X-ray diffractometer (PANalytical Co., Longmont, CO) with a Cu Kα X-ray resource. All the measurements were operated at 45 kV and 40 mA. Samples were scanned from 4 to 90° and the step size was 0.0263°. Surface morphologies of the electro-spun mats were observed by a scanning electron microscope (SEM, Hitachi High Technologies America, Schaumburg, IL). The surface of each sample was sputter-coated with platinum before viewing. The accelerating voltage was selected to be 20 kV. Tensile properties of the electrospun fiber mats were investigated using an AR2000ex rheometer (TA Instruments-Waters LLC, New Castle, DE) with a solid clamp fixture. Three tensile specimens (20 in length and 5 mm in width) were cut from the electrospun mats. The gauge length was 12 mm, and the testing speed was 1.2 mm/min. Mechanical properties, including tensile strength and elongation at break, were calculated based on the measured stress-strain curves.

3. Results and discussions

3.1. Rheological properties of electrospinning solutions

It is well known that the viscosity of electrospinning solutions plays a key role in the morphology and performance of electrospun mats. **Figure 1a** shows the relationship between the viscosity and shear rate for different materials formulated. For pure PEO solution (P100),

http://dx.doi.org/10.5772/intechopen.76392

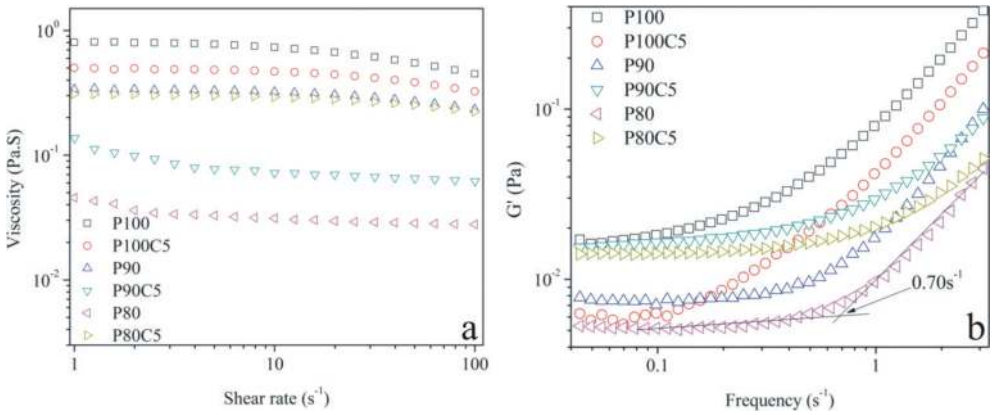

Figure 1. Rheological properties of different suspensions: (a) viscosity-shear rate plot (b) storage modulus-frequency plot from oscillatory measurements.

its viscosity decreased with the increased shear rate, which was attributed to the shear thinning phenomenon [24]. With the addition of PVP and CNCs, the viscosity of the suspensions decreased. For PEO/PVP material, the decrease was attributed to the more viscous nature of PVP. With regard to suspensions that contain CNCs, the decrease was attributed to the interaction between CNCs and PEO. With addition of CNCs, the intra-molecular interaction between PEO molecules was distracted, resulting in the decrease in viscosity. It should be pointed that the viscosity of P80C5 was higher than that of P90C5 and P80, attributed to the special chemical interaction (discussed in the next section).

For oscillatory rheological measurements, the relationship between storage modulus and frequency in the low frequency or terminal region allowed us to evaluate the intermolecular interactions in a multi-component system. If there are certain special chemical interactions (e.g., H-bond interactions) in the tested samples, a so-called "second platform" usually exists [23]. As shown in **Figure 1b**, an obvious platform for P80C5 was observed, which is in a sharp contrast with that for P100 and indicates possible special interactions. To quantitatively compare the length of platform, the extrapolated critical frequency that denotes the frequency at which the substantial increase in storage modulus begins was calculated (e.g., 0.70 s^{-1} for P80 in **Figure 1b**).

P100 showed a critical frequency of 0.29 s^{-1}. With the addition of 5 phr CNCs (P100C5), the critical frequency decreased to 0.11 s^{-1}. Such a decrease was expected, since the hydroxyl groups in CNCs can interact with the ether oxygen in PEO molecules (**Figure 2b**), and therefore distract the intramolecular interactions of PEO (**Figure 2a**) [6]. With the addition of PVP, the critical frequency increased to 0.51 and 0.70 for P90 and P80, respectively, which was attributed to the interaction between carbonyl groups in PVP and hydroxyl groups in PEO (**Figure 2c**). When PVP and CNCs were combined, it is interesting to note that the critical frequency still increased, even considering the fact that CNCs can distract the intramolecular interactions of PEO. This interesting phenomenon was due to the interactions between carbonyl group and hydroxyl groups in CNCs (**Figure 2d**) [22].

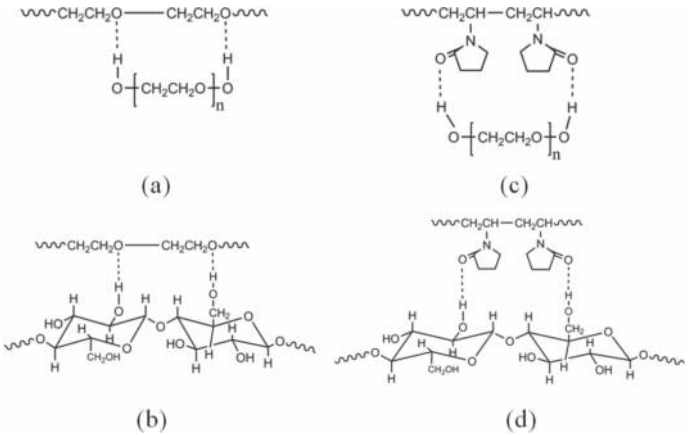

Figure 2. Scheme of interactions between different materials in the composite fibers: (a) PEO/PEO; (b) PEO/PVP; (c) PEO/CNCs; (d) PVP/CNCs.

3.2. FTIR spectra of electrospun mats

FTIR was further used to investigate the proposed interaction and the specific curves are shown in **Figure 3a**. Pure PEO electrospun mat exhibited the absorption bands at 2882, 1467, 1146, 1098, 1060 and 961 cm^{-1}, which were assigned to CH_2 stretching, C–H bending mode and C–O–C stretching vibration, respectively [6]. It should be pointed out that the O–H absorption band was undetectable in FTIR curves. This was due to the high molecular weight of PEO, and therefore the role of its end group (–OH) could be ignored [25]. With the addition of 5 phr CNCs, the absorption band for C–O–C stretching vibration was shifted from 961 to 957 cm^{-1}, suggesting the possible interactions between PEO and CNCs. With respect to PEO/PVP and PEO/PVP/CNCs systems, the main absorption bands were not shifted, but instead new absorption bands assigned to the carbonyl groups in PVP [22] were observed in **Figure 3b**. For P90 and P90C5, the wave number of carbonyl group was located at 1673 cm^{-1}. As the PVP content increased to 20 phr, the peak was shifted to 1669 cm^{-1} for P80 and 1665 cm^{-1} for P80C5, indicating possible interactions existed in these systems [25]. All the FTIR results corresponded well with the abovementioned results of oscillatory rheological tests.

3.3. DSC data of electrospun mats

The effects of CNCs and PVP on the melting and crystallization behaviors of PEO were investigated using the DSC technique. The specific parameters derived from DSC curves, including peak melting, and peak crystallization temperature, melting enthalpy, the half time of crystallization, and crystallinity, are listed in **Table 2**. The crystallinity (X_c) is calculated using the following equation:

$$X_C = \frac{\Delta H_m / \varphi}{\Delta H_m^*} x\ 100\% \quad (1)$$

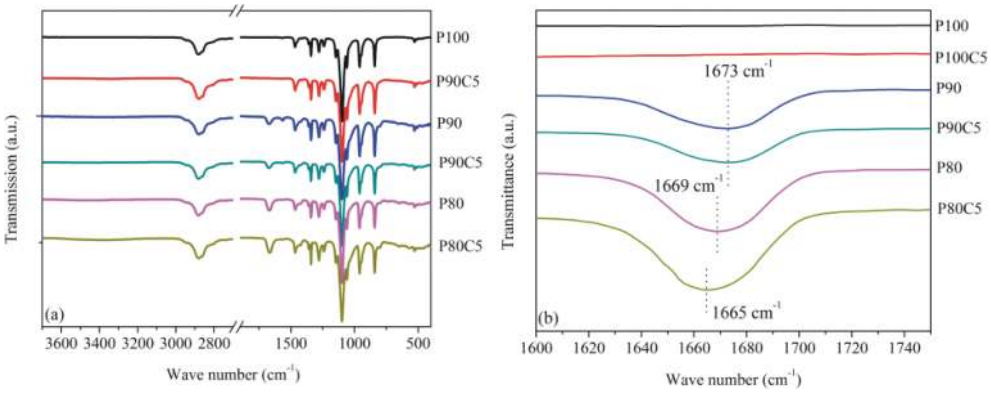

Figure 3. FTIR curves of different electrospun fiber mats: (a) 3700–400 cm^{-1}; (b) 1750–1600 cm^{-1}.

Material type	DSC[a]					TGA[b]			
	T_m^p (°C)	ΔH_m ($J \cdot g^{-1}$)	X_c (%)	T_c^p (°C)	$t_{1/2}$ (min)	T_{onset} (°C)	T_{p1} (°C)	T_{p2} (°C)	Deriv. weight (%/°C)
P100	65.9	157.4	73.7	48.3	0.26	393.5	-	416.6	3.11
P100C5	64.9	141.3	69.5	48.6	0.26	386.9	-	417.2	2.29
P90	64.4	131.4	68.3	47.7	0.27	374.7	-	413.5	1.80
P90C5	63.7	125.3	68.4	49.3	0.20	382.2	278.3	416.5	2.75
P80	64.8	119.6	69.9	48.1	0.26	372.6	288.4	416.7	2.13
P80C5	64.7	120.1	73.9	49.4	0.19	379.9	277.7	419.1	1.83

[a]T_m^p: peak melting temperature; T_c^p: peak crystallization temperature; $t_{1/2}$: the half time of crystallization; ΔH_m: melting enthalpy of PEO; X_c: crystallinity of PEO.

[b]T_{onset} is the temperature corresponding to 10 wt% weight loss; T_{p1} and T_{p2} are the temperature corresponding to the first and the second peak of DTG curve; Deriv. Weight: derive. weight of the second peak of DTG curve.

Table 2. DSC and TGA data of different electrospun PEO-PVP-CNC composite fiber mats systems.

Where ΔH_m is the melting enthalpy derived from the DSC curves, ΔH_m^* = 213.7 J/g [14] is the melting enthalpy when crystallinity of PEO is 100%, and φ is the weight fraction of PEO in the blend and composites.

As shown in **Table 2**, addition of either PVP or CNC decreased the T_m^p and the ΔH_m of PEO. These decreases can be accounted by the possible interactions between different components with PEO. And the slight decrease in T_m^p indicated that the crystallite size of PEO became smaller [26]. With regard to crystallinity, mere incorporation of PVP and CNCs into PEO did cause decrease in X_c. For example, the X_c for P100 decreased from 73.7 to 69.5% and 69.9 for P100C5 and P80, respectively. However, it is interesting to note that similar decrease in X_c did not occur when CNCs and PVP were combined. The X_c of P80C5 was 73.9%, which was even higher than that of P100. This result might be in conflict with the possible interactions observed in the

abovementioned oscillatory rheological measurements and FTIR results, since special interactions usually hinders the crystallization and results in a decreasing crystallinity [26]. Similar interesting results were also observed regarding the crystallization behaviors. As shown in **Table 2**, either PVP or CNCs did not change $t_{1/2}$. However, the T_c^p values of P90C5 and P80C5 were shifted to higher temperature while their $t_{1/2}$ value were reduced, indicating that the nucleating effect occurred [27]. These unexpected results in ternary composite system, including the increased crystallinity, and the nucleating effect, were responsible for the improved mechanical performance.

3.4. Thermal stability data of electrospun mats

The effects of PVP and CNCs on the thermal stability of the composite fibers were investigated by TG analysis. The relevant parameters derived are summarized in **Table 2**. Pure PEO nanofibers exhibited one-step degradation with T_{onset} of 393.5°C. With the addition of PVP, the blend (P90) still exhibited one-degradation step, but the T_{onset} decreased considerably. This is due to the relative lower thermal stability of PVP. When CNCs were added, two-step degradation was observed for all the prepared composites, which were assigned to the degradation of CNCs and polymer/blends, respectively. Incorporation of CNCs to the P100 system decreased the T_{onset} values (P100C5). Surprisingly, the addition of CNCs slightly increased the T_{onset} values of P90C5 and P80C5 in comparison with these for P90 and P80, indicating that CNCs even played a positive role in enhancing the initial thermal stability of the P90 and P80 systems. This improvement might be due to the enhanced crystallinity of P90C5 and P80C5 [9]. The peak height of the second peak on the DTG curves decreased with the addition of either PVP or CNCs. This was due to the dilution effect [28, 29] and indicated that the addition of other components could enhance the overall thermal stability of PEO, even though they did decrease the initial thermal stability (T_{onset}).

3.5. Crystalline structure of electrospun mats

XRD was used to investigate the crystal structures of the nanofibers. The diffraction patterns are shown in **Figure 4**. The crystallite size was calculated using the Scherrer equation as follows [6]:

$$L = \frac{K\lambda}{B}\cos\theta \tag{2}$$

where λ is 1.54 Å (the wavelength of Cu K α X-ray), K is 0.89 and B is the full width at half maximum of diffraction peaks. Pure PEO nanofibers exhibited two diffraction peaks at 19° and 23°, which were assigned to the diffraction of the (120, 112) crystal plane [14], respectively. With the addition of PVP and CNC, no shift in the diffraction peak was observed for P80 and P80C5, indicating that the crystal type did not change. However, the crystallite size of (120) plane decreased from 371 Å for P100 to 337 Å for P80C5. This decrease in crystallite size corresponded well with the abovementioned decreasing T_m^p observed in DSC tests.

http://dx.doi.org/10.5772/intechopen.76392

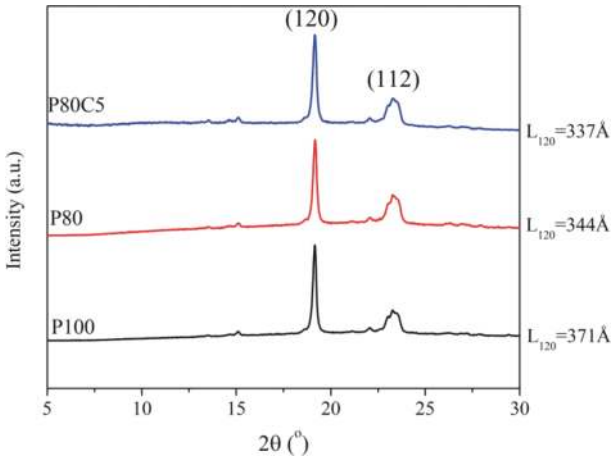

Figure 4. XRD results of different electrospun fiber mats.

3.6. Tensile properties of electrospun mats

The tensile properties, including tensile strength, elongation at break and fracture toughness, are summarized in **Figure 5**. As shown in **Figure 5a**, addition of either PVP or CNCs did have a limited reinforcing effect on PEO. For example, the tensile strength increased from 1.59 MPa (P100) to 1.94 MPa (P100C5) and 2.26 MPa (P80), respectively. Surprisingly, when 20 phr PVP and 5 phr CNCs were combined, an impressive reinforcing effect was achieved. The tensile strength increased to 3.17 MPa, which was nearly a one-fold increase. For elongation at break (**Figure 5b**), addition of PVP and CNCs resulted in a slight decrease. This decline was expected, since the increased rigidity was often accompanied with loss in ductility [9]. With regard to the fracture toughness (**Figure 5b**), all samples exhibited a slight decrease except P80C5. The fracture toughness of P80C5 increased from 223 to 320 kJ/m^2. This was due to the higher strength value of P80C5 (the fracture toughness is proportional with the area under the stress-strain curves) and indicated that the combination of 20 phr PVP and 5 phr CNCs could simultaneously reinforce and toughen PEO.

3.7. Morphology of electrospun mats

The morphologies of different electro-spun mats are shown in **Figure 6**. For pure PEO (P100), the nanofibers combined with some beads were observed, which is different from the homogeneous nanofibers reported in other literatures [6, 14]. This difference is believed to be due to the lower concentrations of PEO used in this work, based on which the entanglement between different macromolecules was low and therefore resulted in some fiber-bead-fiber morphology after electrospinning process [30]. With the addition of CNCs and PVP, more beads were introduced. For the composite systems, addition of CNCs distracted the interactions between PEO molecules, which results in the lower entanglement between PEO molecules. With

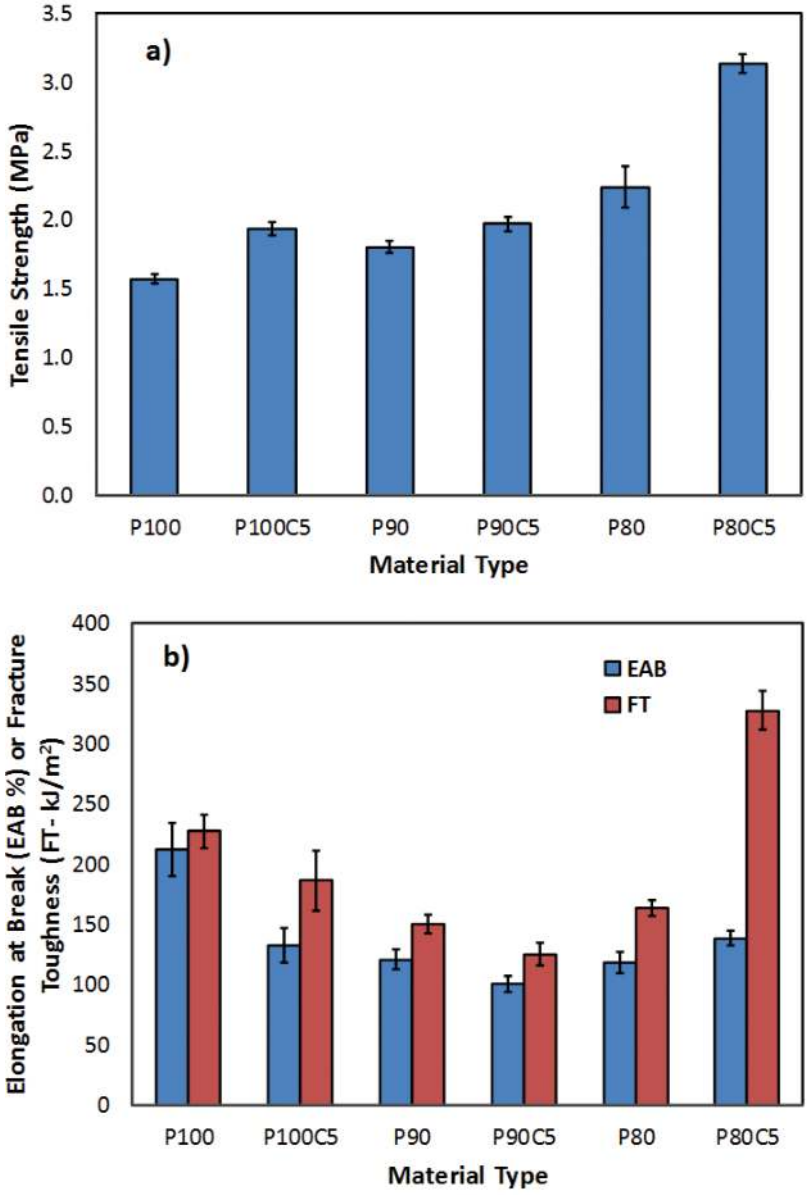

Figure 5. Mechanical properties of different electrospun fiber mats: (a) tensile strength and (b) elongation at break and fracture toughness.

regard to systems that contain PVP, its low molecular weight and low electrospinning nature accounted for the formation of the bead morphology [31]. The electrospun mats with fiber-bead-fiber morphology exhibited the highest mechanical performance as discussed earlier.

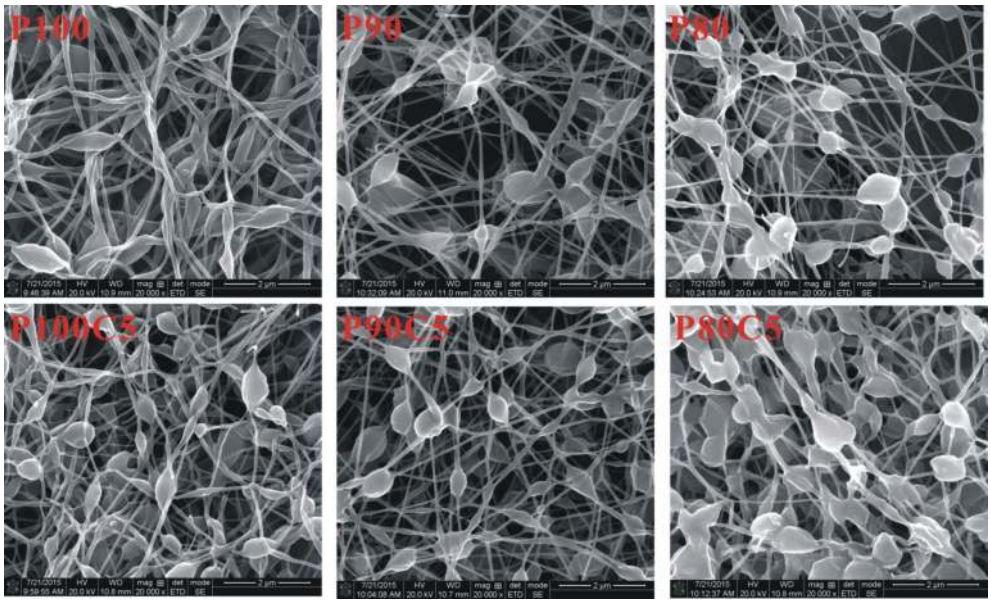

Figure 6. SEM images of different electro-spun fiber mats.

To better elucidate the role of beads played in the fiber reinforcement, the morphology of P80C5 before and after tensile test was obtained (**Figure 7**). The nanofibers were highly orientated along the tensile stress direction (the horizontal direction). It is interesting to note that the number of the beads became smaller and the shape of the beads was highly elongated under stress. This indicated that the beads worked as stress concentrators, and they were elongated, helped dissipate the applied energy, and therefore resulted in overall composite strength reinforcement.

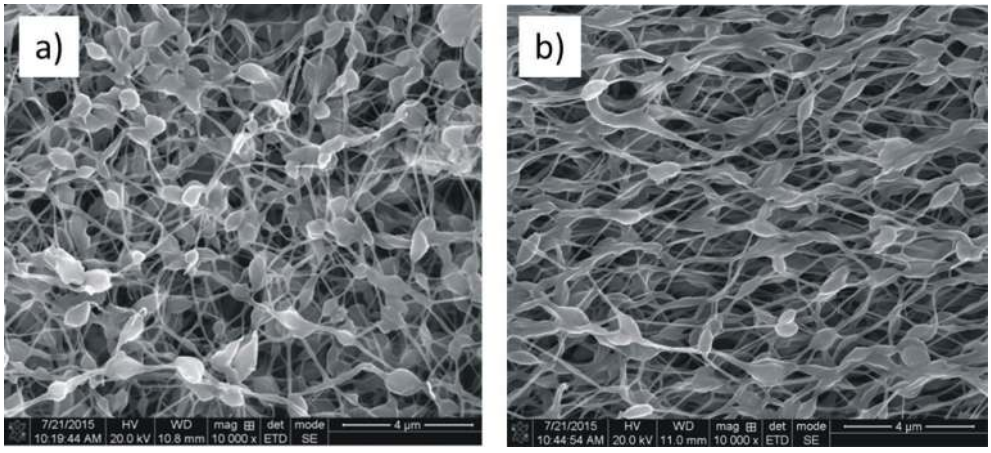

Figure 7. SEM images of the P80C5 composite fiber mat before and after tensile test.

3.8. Discussion on reinforcing mechanisms

There are many factors that determine whether a reinforcing effect can be achieved in the composite fibers. Based on the abovementioned results, the reinforcing mechanism is proposed and its schematic presentation is shown in **Figure 8**. There are three possible factors that contribute to the reinforcement.

The first factor is the crystallinity. For semi-crystalline polymers like PEO, its mechanical strength is proportional with its crystallinity. Herein, in comparison with that of 69.9% for P80, the crystallinity of P80C5 was 73.9%, which was almost the same as that for P100 (73.7%). The reason for the increase in crystallinity is the interaction between PVP and CNCs. For P80, the PVP chains entangled with PEO chains in amorphous region (**Figure 8a**). When 5 phr CNCs was introduced, the CNCs interacted with PVP, and helped free some PEO amorphous chains from the interaction with PVP. As a result, the freed PEO chains were rearranged into crystal lattice and therefore contributed to a higher crystallinity (**Figure 8b**) and the synergistic reinforcing effect. This assumption was verified by comparing the FTIR

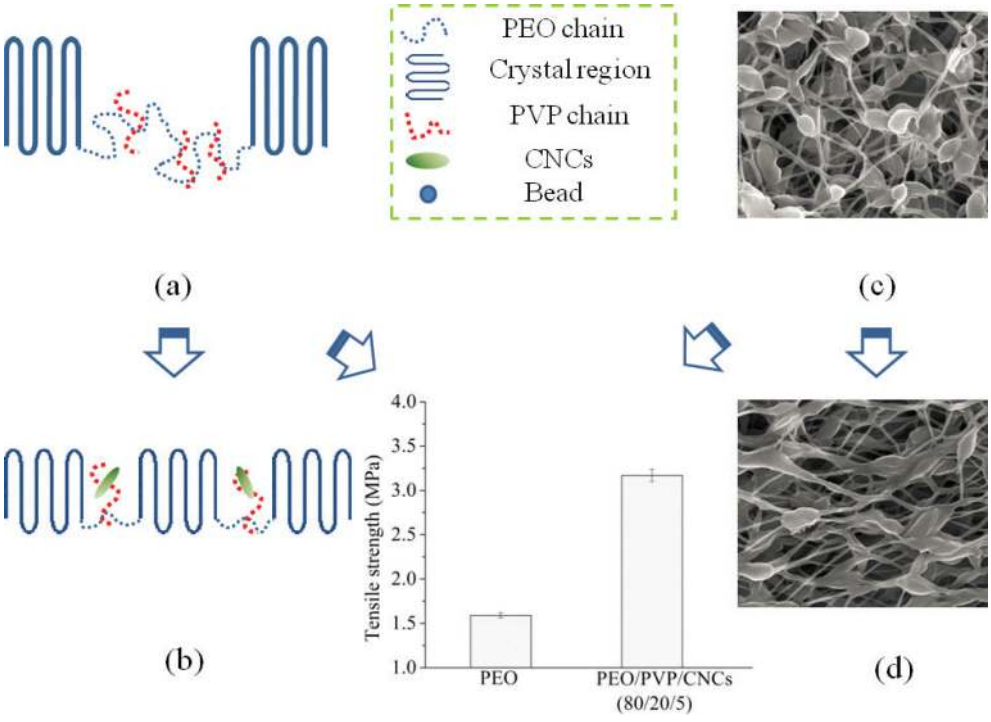

Figure 8. Schematic presentation of reinforcing mechanism: (a) P80 system; (b) P80C5 system; (c) fiber-bead-fiber morphology before tensile testing; (d) fiber-bead-fiber morphology after tensile testing.

results of P80 and P80C5, since the characteristic peak of carbonyl group of PVP was shifted to lower wave number, while all other characteristic peaks of PEO remained the same. In addition, the number of carbonyl group in PVP was considerably higher than the hydroxyl group (end group) in PEO. Therefore, CNCs were more prone to interact with PVP rather than PEO in general.

The second factor is related to the unique fiber-bead-fiber morphology of the prepared fiber mats. For P80C5, both the number and the size of the beads were the largest (**Figure 5**). And under the tensile loading, the beads were highly oriented and elongated along the tensile force direction (**Figure 8**). The elongation process of the beads (**Figure 8c** and **8d**) helped dissipate the applied energy. As a result, a surprising reinforcement was achieved. The third factor is due to the nature of CNCs and PVP. Both of them had a higher rigidity than that of PEO, which also accounted for the observed reinforcement.

It should be pointed out that the presence of spherical beads or elongated shape objects in electrospun fibers are often considered as defects in the manufactured materials [32, 33]. This could be due to the lower concentration of PEO, and the use of CNCs and PVP in the system. Further studies are needed to establish the reinforcing effect of combined CNCs and PVP in un-beaded electrospun fibers.

4. Conclusions

PVP and CNCs were used as reinforcement materials in electrospun PEO fiber mats. Addition of PVP and/or CNCs improved the overall thermal stability and mechanical properties of the PEO fibers. A synergistic reinforcing effect was observed when 20 phr PVP and 5 phr CNCs were used. Addition of CNCs induced special interactions with PVP and therefore disentangled the PVP and PEO chains. The freed PEO chains were rearranged into crystal lattice and contributed to a higher crystallinity as verified by the DSC results. In addition, the synergistic reinforcing effect was also accompanied with a fiber-bead-fiber morphology. Under the tensile loading, the beads were orientated and elongated, which helped dissipate more applied energy and therefore resulted in improved mechanical performance of the composites. This work demonstrates a new approach for reinforcing electrospun PEO-based composite fibers for sustainable green composite development.

Acknowledgements

We acknowledge the support from the Louisiana Board of Regents LEQSF(2017-18)-RD-A-01], Nanjing Forestry University (Nanjing, China), and Henan Academy of Science (Zhengzhou, China).

Author details

Qinglin Wu[1]*, Changtong Mei[2], Xiuqiang Zhang[3], Tingzhou Lei[3], Zhen Zhang[1] and Meichun Li[1]

*Address all correspondence to: wuqing@lsu.edu

1 School of Renewable Natural Resources, Louisiana State University, Baton Rouge, LA, USA

2 College of Materials Science and Engineering, Nanjing Forestry University, Jiangsu, China

3 Key Biomass Energy Laboratory of Henan Province, Zhengzhou, Henan, China

References

[1] Xu H, Xie L, Jiang X, Hakkarainen M, Chen J-B, Zhong G-J, Li Z-M. Structural basis for unique hierarchical cylindries induced by ultrahigh shear gradient in single natural fiber reinforced poly(lactic acid) green composites. Biomacromolecules. 2014;**15**(5):1676-1686. DOI: 10.1021/bm500100z

[2] Chen J, Lu L, Wu D, Yuan L, Zhang M, Hua J, Xu J. Green poly(e-caprolactone) composites reinforced with electrospun polylactide/poly(e-caprolactone) blend fiber mats. ACS Sustainable Chemistry & Engineering. 2014;**2**(9):2012-2110. DOI: 10.1021/sc500344n

[3] Sun Q, Mandalika A, Elder T, Nair SS, Meng X, Huang F, Ragauskas AJ. Nanocomposite film prepared by depositing xylan on cellulose nanowhiskers matrix. Green Chemistry. 2014;**16**(7):3458-3462. DOI: 10.1039/C4GC00793J

[4] Bodros E, Pillin I, Montrelay N, Baley C. Could biopolymers reinforced by randomly scattered flax fibre be used in structural applications? Composites Science and Technology. 2007;**67**(3-4):462-470

[5] Mohanty AK, Misra M, Drzal LT. Sustainable bio-composites from renewable resources: Opportunities and challenges in the green materials world. Journal of Polymers and the Environment. 2002;**10**(1-2):19-26. DOI: https://doi.org/10.1016/j.compscitech.2006.08.024

[6] Zhou C, Chu R, Wu R, Wu Q. Electrospun polyethylene oxide/cellulose nanocrystal composite nanofibrous mats with homogeneous and heterogeneous microstructures. Biomacromolecules. 2011;**12**(7):2617-2625. DOI: 10.1021/bm200401p

[7] Zhang Z, Zhao X, Zhang J, Chen S. Effect of nano-particles-induced phase inversion on largely improved impact toughness of PVC/α-methylstyrene–acrylonitrile copolymer (α-MSAN)/CPE-matrix composites. Composites Science and Technology. 2013;**86**:122-128. DOI: https://doi.org/10.1016/j.compscitech.2013.07.009

[8] Zhou C, Shi Q, Guo W, Terrell L, Qureshi AT, Hayes DJ, Wu Q. Electrospun bio-nanocomposite scaffolds for bone tissue engineering by cellulose nanocrystals reinforcing maleic anhydride grafted PLA. ACS Applied Materials & Interfaces. 2013;**5**(9):3847-3854. DOI: 10.1021/am4005072

[9] Zhang Z, Wu Q, Song K, Ren S, Lei T, Zhang Q. Using cellulose Nanocrystals as a sustainable additive to enhance hydrophilicity, mechanical and thermal properties of poly(vinylidene fluoride)/poly(methyl methacrylate) blend. ACS Sustainable Chemistry & Engineering. 2015;**3**(4):574-582. DOI: 10.1021/sc500792c

[10] Zhang Z, Wu Q, Song K, Lei T, Wu Y. Poly(vinylidene fluoride)/cellulose nanocrystals composites: Rheological, hydrophilicity, thermal and mechanical properties. Cellulose. 2015;**22**(4):2431-2441. DOI: 10.1007/s10570-015-0634-y

[11] Sun Q, Foston M, Sawada D, Pingali S, O'Neill H, Li H, Wyman C, Langan P, Pu Y, Ragauskas A. Comparison of changes in cellulose ultrastructure during different pretreatments of poplar. Cellulose. 2014;**21**(4):2419-2431. DOI: 10.1007/s10570-014-0303-6

[12] Azizi Samir MAS, Alloin F, Sanchez J-Y, Dufresne A. Cellulose nanocrystals reinforced poly(oxyethylene). Polymer. 2004;**45**(12):4149-4157. DOI: 10.1016/j.polymer.2004.03.094

[13] Xu X, Liu F, Jiang L, Zhu JY, Haagenson D, Wiesenborn DP. Cellulose nanocrystals vs. cellulose nanofibrils: A comparative study on their microstructures and effects as polymer reinforcing agents. ACS Applied Materials & Interfaces. 2013;**5**(8):2999-3009

[14] Xu X, Wang H, Jiang L, Wang X, Payne SA, Zhu JY, Li R. Comparison between cellulose nanocrystal and cellulose nanofibril reinforced poly(ethylene oxide) nanofibers and their novel shish-kebab-like crystalline structures. Macromolecules. 2014;**47**(10):3409-3416. DOI: 10.1021/am302624t

[15] Zhou Y, Qi P, Zhao Z, Liu Q, Li Z. Fabrication and characterization of fibrous HAP/PVP/PEO composites prepared by sol-electrospinning. RSC Advances. 2014;**4**(32):16731-16738. DOI: 10.1039/C3RA47168C

[16] Talebian S, Mehrali M, Mohan S, Balaji Raghavendran HR, Mehrali M, Khanlou HM, Kamarul T, Afifi AM, Abass AA. Chitosan (PEO)/bioactive glass hybrid nanofibers for bone tissue engineering. RSC Advances. 2014;**4**(90):49144-49152. DOI: 10.1039/C4RA06761D

[17] Cheng F, Gao J, Wang L, Hu X. Composite chitosan/poly(ethylene oxide) electrospun nanofibrous mats as novel wound dressing matrixes for the controlled release of drugs. Journal of Applied Polymer Science. 2015;**132**(24). DOI: 10.1002/app.42060

[18] Aliabadi M, Irani M, Ismaeili J, Piri H, Parnian MJ. Electrospun nanofiber membrane of PEO/chitosan for the adsorption of nickel, cadmium, lead and copper ions from aqueous solution. Chemical Engineering Journal. 2013;**220**:237-243. DOI: 10.1016/j.cej.2013.01.021

[19] Liu X, Xu Y, Wu Z, Chen H. Poly(N-vinylpyrrolidone)-modified surfaces for biomedical applications. Macromolecular Bioscience. 2013;**13**(2):147-154. DOI: 10.1002/mabi.201200269

[20] Cheng J, Wang S, Chen S, Zhang J, Wang X. Crystallization behavior and hydrophilicity of poly(vinylidene fluoride)/poly(methyl methacrylate)/poly(vinylpyrrolidone) ternary blends. Polymer International. 2012;**61**(3):477-484. DOI: 10.1002/pi.3185

[21] Pei A, Zhou Q, Berglund LA. Functionalized cellulose nanocrystals as biobased nucleation agents in poly(l-lactide) (PLLA)—Crystallization and mechanical property effects.

Composites Science and Technology. 2010;**70**(5):815-821. DOI: https://doi.org/10.1016/j.compscitech.2010.01.018

[22] Taylor L, Zografi G. Spectroscopic characterization of interactions between PVP and indomethacin in amorphous molecular dispersions. Pharmaceutical Research. 1997; **14**(12):1691-1698

[23] Song P, Xu Z, Guo Q. Bioinspired strategy to reinforce PVA with improved toughness and thermal properties via hydrogen-bond self-assembly. ACS Macro Letters. 2013;**2**(12):1100-1104. DOI: 10.1021/mz4005265

[24] Zhang Z, Wang S, Zhang J. Large stabilizing effect of titanium dioxide on photodegradation of PVC/α-methylstyrene-acrylonitrile copolymer/impact modifier-matrix composites. Polymer Composites. 2014;**35**(12):2365-2375. DOI: 10.1002/pc.22904

[25] Pielichowska K, Głowinkowski S, Lekki J, Biniaś D, Pielichowski K, Jenczyk J. PEO/fatty acid blends for thermal energy storage materials. Structural/morphological features and hydrogen interactions. European Polymer Journal. 2008;**44**(10):3344-3360

[26] Li J, Lai MF, Liu JJ. Control and development of crystallinity and morphology in poly(β-hydroxybutyrate-co-β-hydroxyvalerate)/poly(propylene carbonate) blends. Journal of Applied Polymer Science. 2005;**98**(3):1427-1436. DOI: 10.1002/app.22117

[27] Zhang Z, Song K, Li Y, Wu Q. Non-isothermal crystallization of poly (vinylidene fluoride)/poly (methyl methacrylate)/cellulose nanocrystal nanocomposites. International Journal of Polymer Analysis and Characterization. 2014;**19**(4):332-341. DOI: https://doi.org/10.1080/1023666X.2014.902530

[28] Zhang Z, Chen S, Zhang J, Li B, Jin X. Influence of chlorinated polyethylene on poly (vinyl chloride)/poly (α-methylstyrene-acrylonitrile) blends: Mechanical properties, morphology and thermal properties. Polymer Testing. 2010;**29**(8):995-1001. DOI: https://doi.org/10.1016/j.polymertesting.2010.09.003

[29] Zhang Z, Li B, Chen S, Zhang J, Jin X. Poly (vinyl chloride)/poly (α-methylstyrene–acrylonitrile)/acrylic resin ternary blends with enhanced toughness and heat resistance. Polymers for Advanced Technologies. 2012;**23**(3):336-342. DOI: 10.1002/pat.1876

[30] Fong H, Chun I, Reneker DH. Beaded nanofibers formed during electrospinning. Polymer. 1999;**40**(16):4585-4592. DOI: https://doi.org/10.1016/S0032-3861(99)00068-3

[31] Gupta P, Elkins C, Long TE, Wilkes GL. Electrospinning of linear homopolymers of poly(methyl methacrylate): Exploring relationships between fiber formation, viscosity, molecular weight and concentration in a good solvent. Polymer. 2005;**46**(13):4799-4810. DOI: https://doi.org/10.1016/j.polymer.2005.04.021

[32] Frenot A, Chronakis IS. Polymer nanofibers assembled by electrospinning. Current Opinion in Colloid & Interface Science. 2003;**8**(1):64-75. DOI: https://doi.org/10.1016/S1359-0294(03)00004-9

[33] Deitzel JM, Kleinmeyer J, Harris DEA, Tan NB. The effect of processing variables on the morphology of electrospun nanofibers and textiles. Polymer. 2001;**42**(1):261-272. DOI: 10.1016/S0032-3861(00)00250-0